united nations
educational, scientific
and cultural
organization

international atomic
energy agency

the
abdus salam
international centre for theoretical physics

ICTP 40th Anniversary

SCHOOL ON SYNCHROTRON RADIATION AND APPLICATIONS
In memory of J.C. Fuggle & L. Fonda

19 April - 21 May 2004

Miramare - Trieste, Italy

1561/23

Inelastic X-ray scattering from electronic excitations

M. Krisch

strada costiera, 11 - 34014 trieste italy - tel. +39 040 2240111 fax +39 040 224163 - sci_info@ictp.trieste.it - www.ictp.trieste.it

Inelastic X-ray scattering from electronic excitations

Michael Krisch
European Synchrotron Radiation Facility
Grenoble, France

krisch@esrf.fr

Introduction
Some theoretical background
Experimental aspects

X-ray Raman scattering
Resonant inelastic X-ray scattering

Fluorescence spectroscopy under high pressure

(Trieste, 14. May 2004)

Inelastic X-ray Scattering

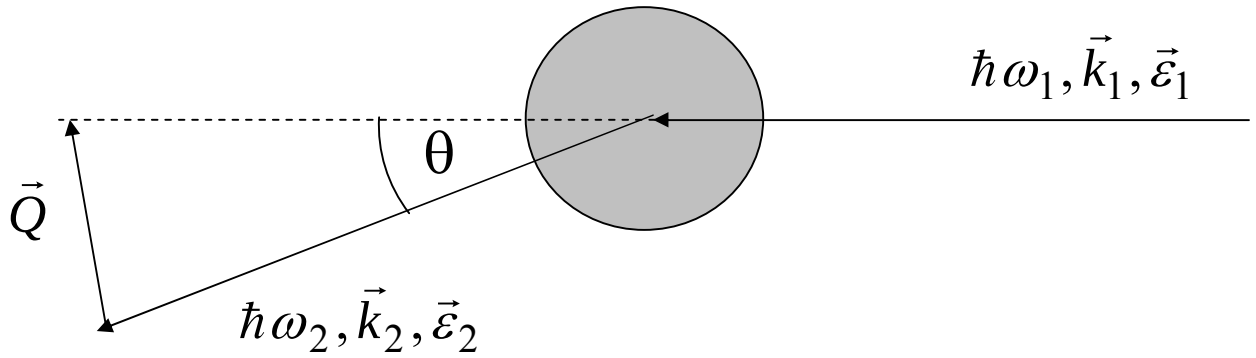

Energy transfer:	$\hbar\omega_1 - \hbar\omega_2$
Momentum transfer:	$\hbar\vec{k}_1 - \hbar\vec{k}_2$

Schematic inelastic x-ray spectrum

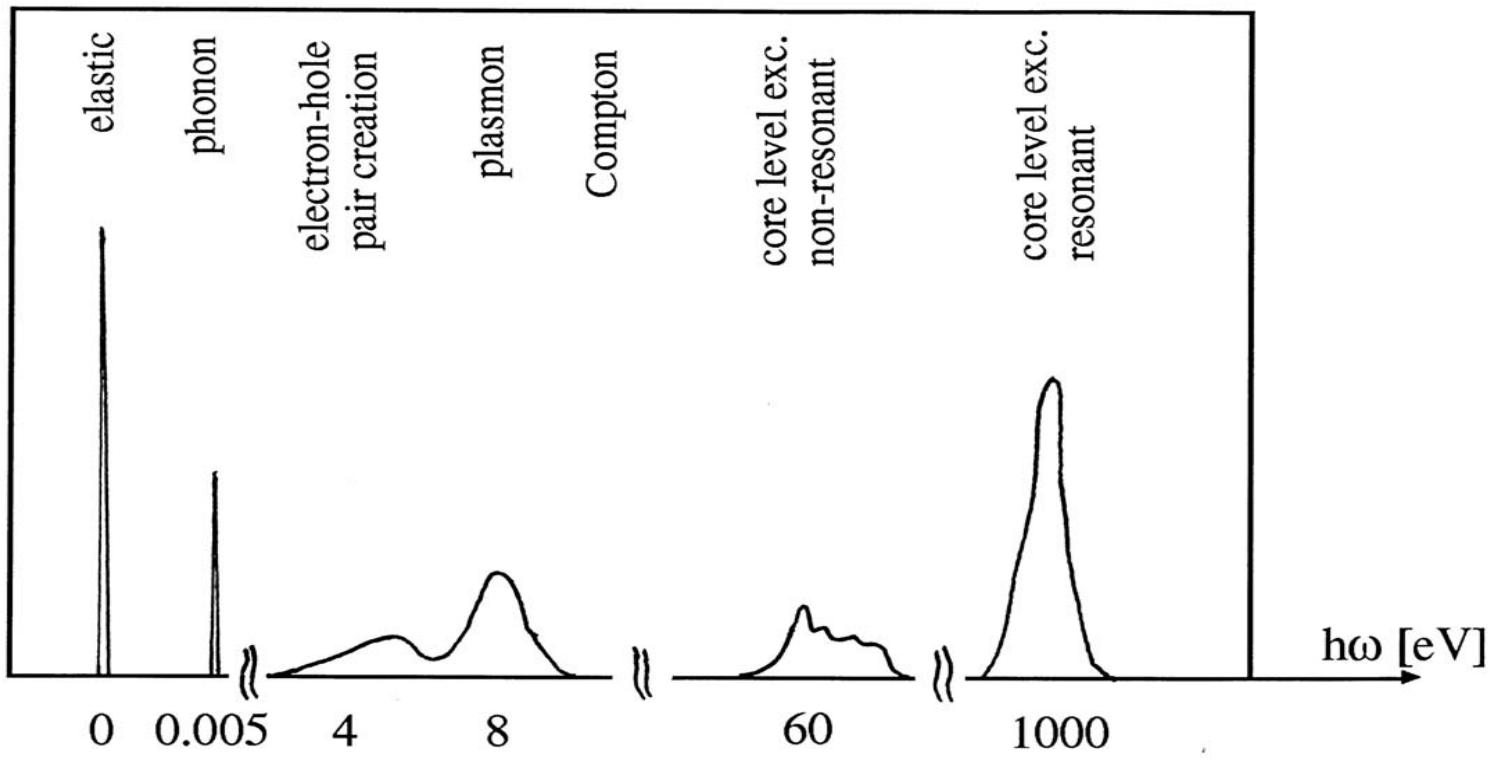

Energy Transfer [eV]

Why IXS from electronic excitations ?

Complementary to other core- and valence level spectroscopies

- (Soft) x-ray absorption spectroscopy (dichroism)
- Photoemission
- Electron energy loss

- element, valence, orbital and spin-selectivity
- bulk sensitivity
- extreme conditions (high pressure)

Photon-electron interaction

$$H_{\text{int}} = \frac{e}{m_e c} \sum_j \left(\frac{e}{2c} \vec{\mathbf{A}}_\mathbf{j}^2 + \vec{\mathbf{A}}_\mathbf{j} \vec{\mathbf{p}}_\mathbf{j} \right)$$

j is the summation over the electrons of the scattering system.

1) Absorption of a photon ($\mathbf{p}\cdot\mathbf{A}$ in 1. Order)

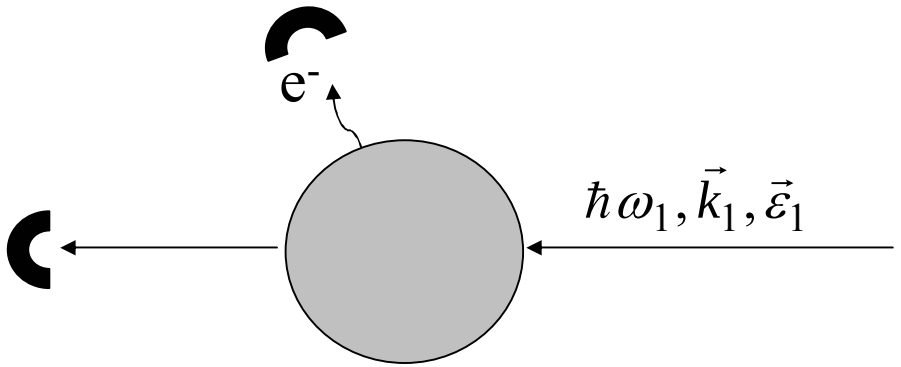

Photon-electron interaction

2) Scattering of a photon (**A·A** in 1. Order)

- non-resonant

3) Scattering of a photon (**p·A** in 2. Order)

- resonant scattering
- absorption followed by emission

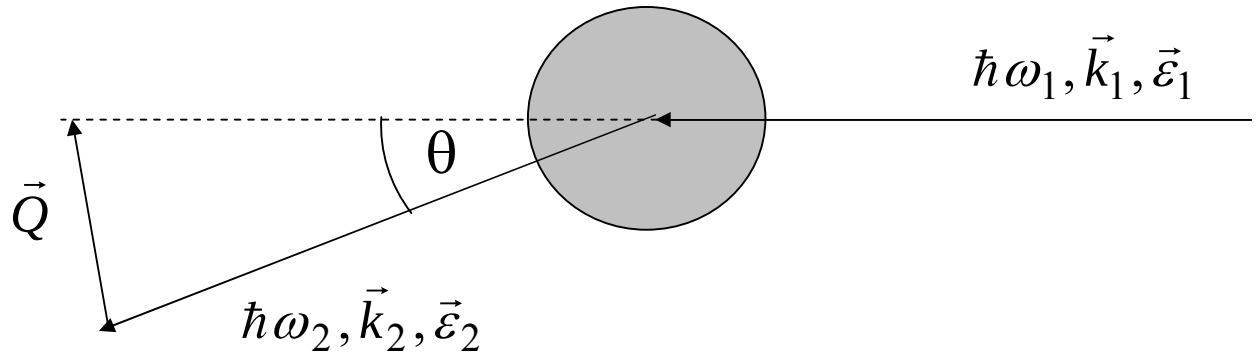

Experimental Setup (ID16 at ESRF)

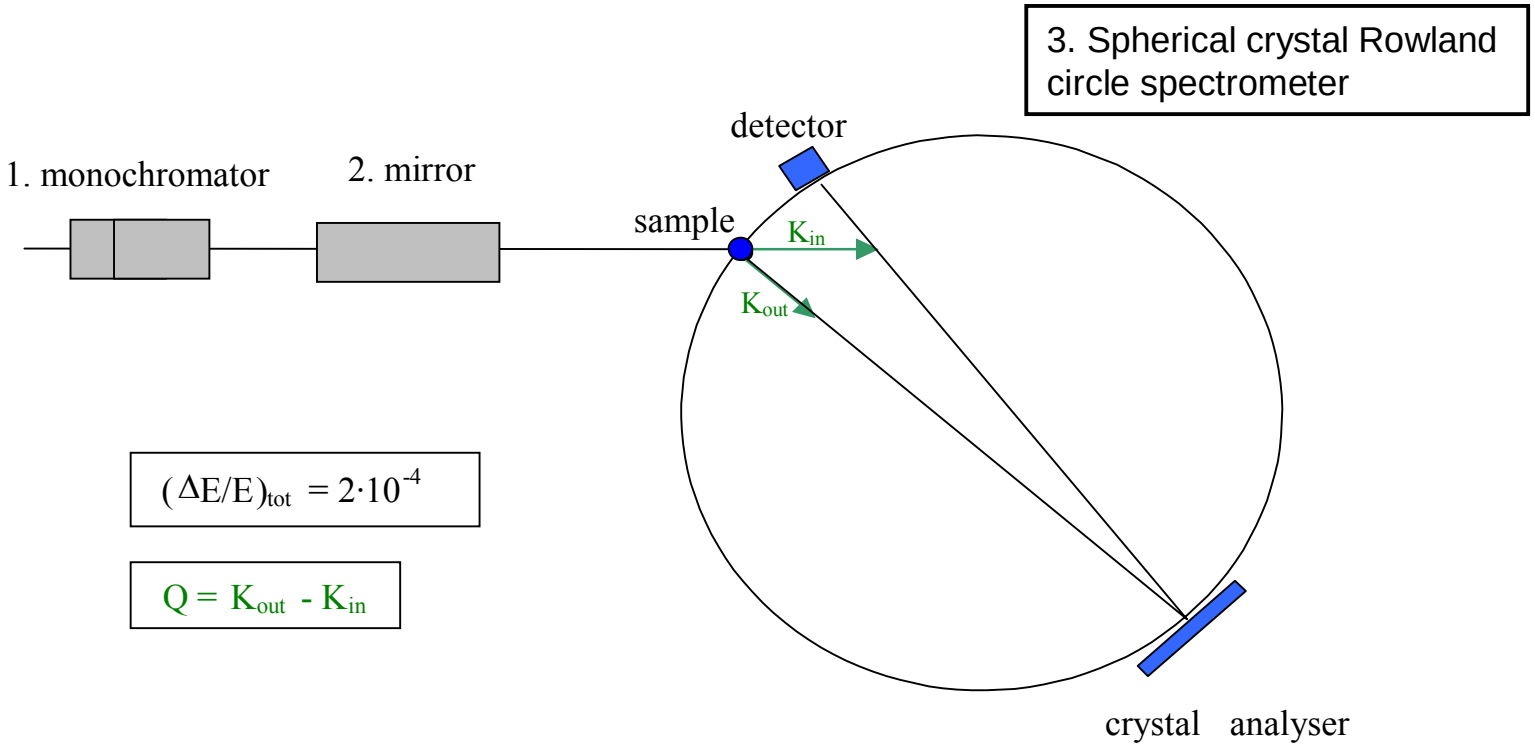

1. Si (111) scanning double crystal monochromator.
2. Toroidal mirror to produce small focal spot at sample.
3. Crystal spectrometer to energy analyze the scattered photons:
   1m spherical crystal, typically Si (440) to Si (555) at Bragg angles 65º - 90º.

Scanning modes

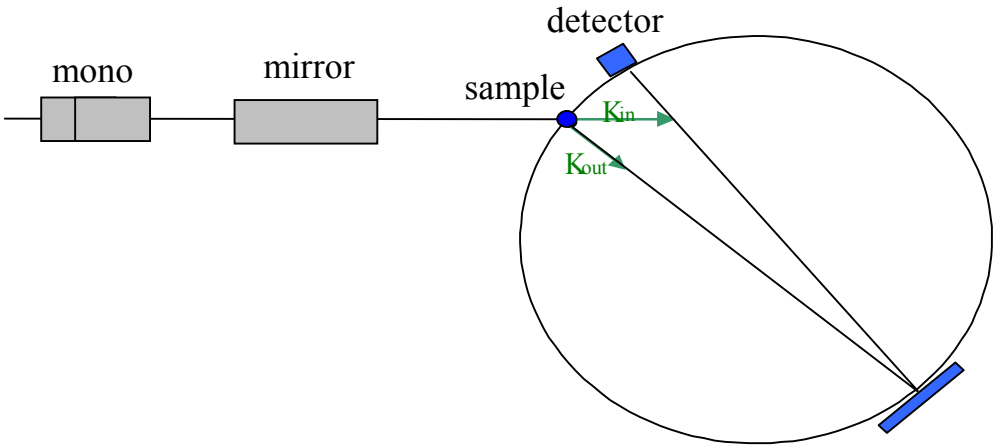

1. $h\omega_2$ fixed, scanning $h\omega_1$	non-resonant IXS, RIXS
2. $h\omega_1$ fixed, scanning $h\omega_2$ (rotating crystal and follow with the detector)	RIXS
3. Scanning $h\omega_1$ and $h\omega_2$ (keeping energy transfer constant)	RIXS

X-ray Raman scattering

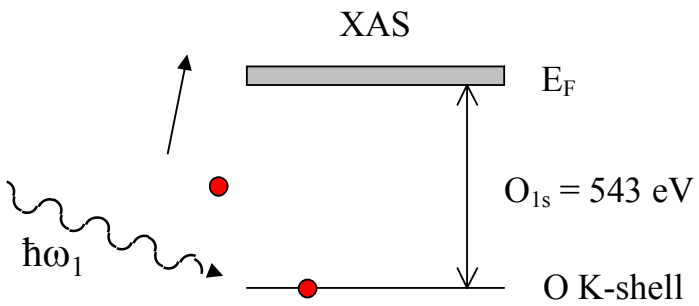

$$E_{1s} + e_k = \hbar\omega_1$$

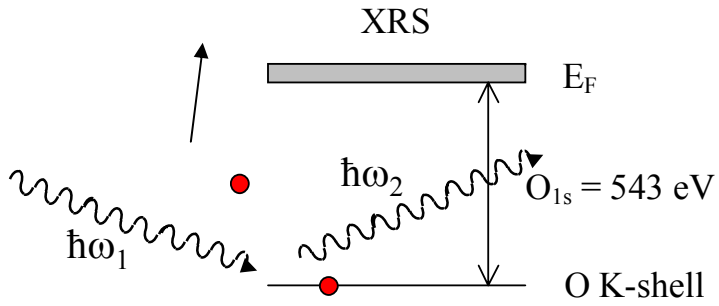

$$E_{1s} + e_k = \hbar\omega = \hbar\omega_1 - \hbar\omega_2$$

Role of incident photon energy in XAS is played by the energy transfer in XRS

=>

certain freedom in the choice of the incident photon energy

Hard X-rays => Bulk sensitivity; Access to buried layers
High pressure and/or temperature

X-ray absorption cross section (dipolar approximation):

$$\frac{d\sigma}{d\omega_1} = 4\pi^2 \alpha \hbar \omega_1 \sum_F \left| \langle F | \vec{\varepsilon}_1 \cdot \vec{r} | I \rangle \right|^2 \delta(E_F - E_I - \hbar\omega_1)$$

X-ray Raman cross section:

$$\frac{d^2\sigma}{d\omega_2 d\Omega} = r_0^2 \frac{\omega_2}{\omega_1} (\vec{\varepsilon}_1 \cdot \vec{\varepsilon}_2) \sum_F \left| \langle F | \sum_j e^{i\vec{Q}\vec{r}_j} | I \rangle \right|^2 \delta(E_F - E_I - \hbar\omega)$$

$Qr << 1$: $e^{iQr} \approx 1 + iQr$

Dipolar regime: identical to photon absorption, where **Q** plays the role of the photon polarization vector ε_1.

$Qr > 1$: e^{iQr}

Multipolar regime: monopolar, dipolar and quadrupolar transitions possible.

XRS from the O K-edge in water and ice

Motivation: probe element-specific local atomic structure in disordered systems

Alternative techniques:

- (Isotopic substitution) neutron scattering
- X-ray (anomalous) scattering

- XANES and EXAFS

Complete IXS spectrum

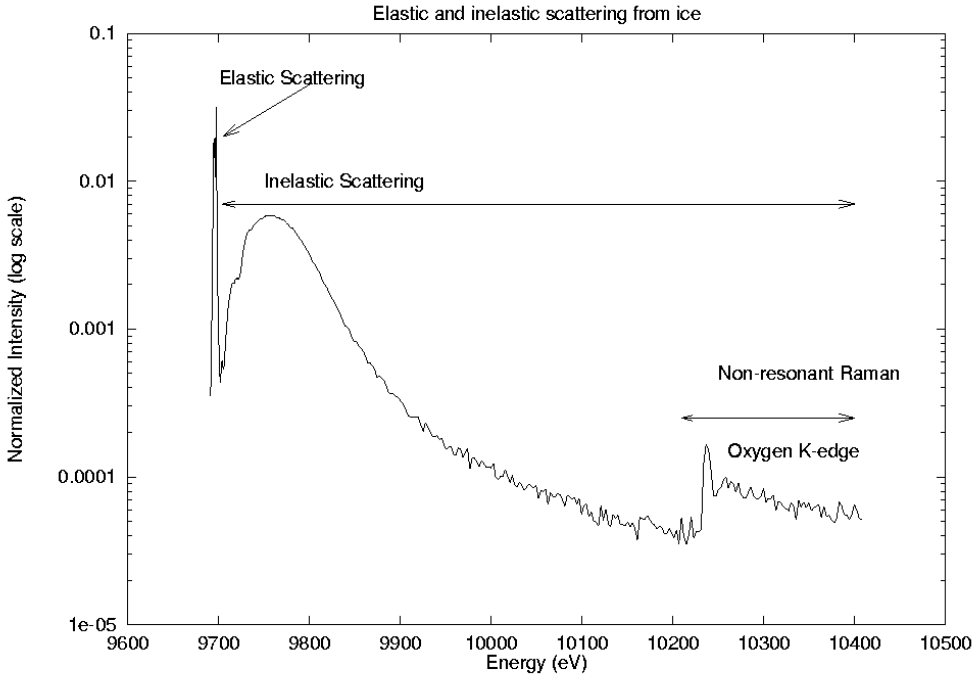

$h\omega_2 = 9686$ eV

$\Delta E = 2$ eV

$Q = 4.38\ A^{-1}$ ($Qr = 0.29$)

$k < 7\ A^{-1}$

XRS Near-edge spectrum of O K-edge

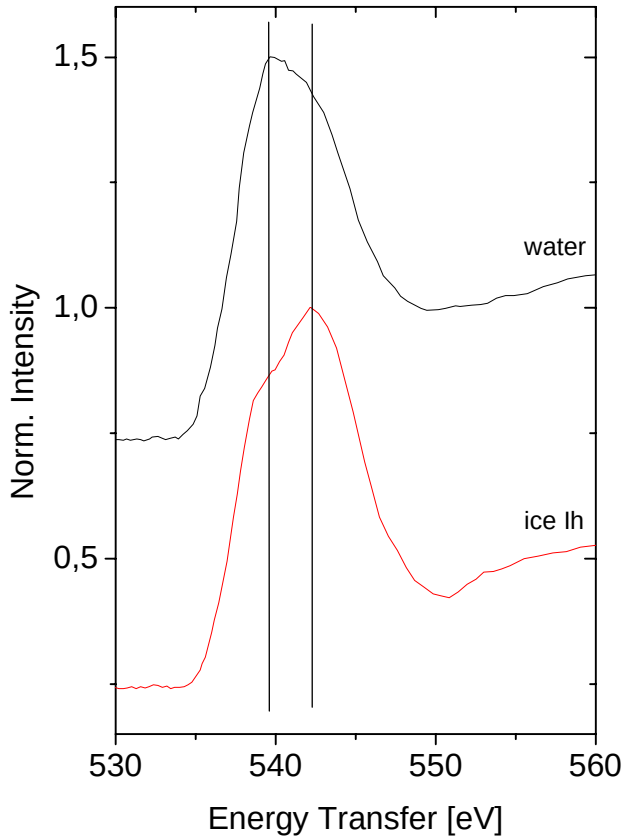

EXAFS Analysis

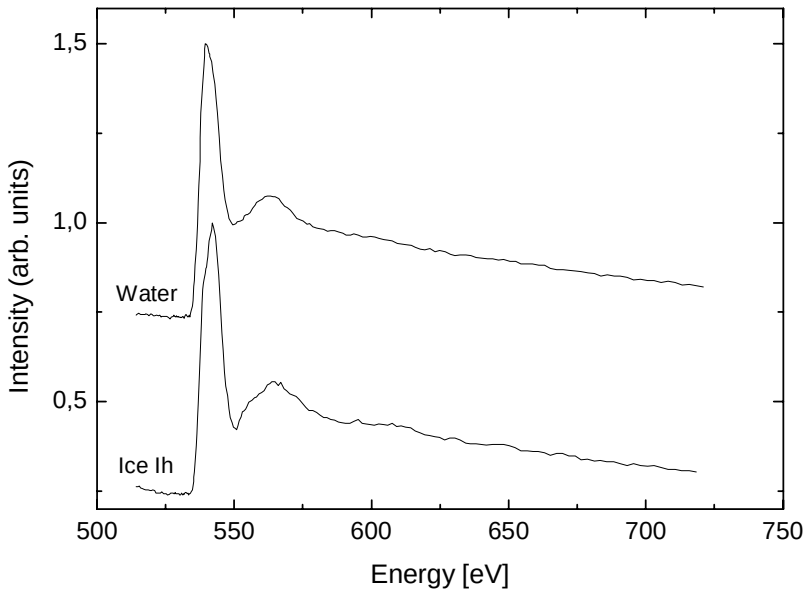

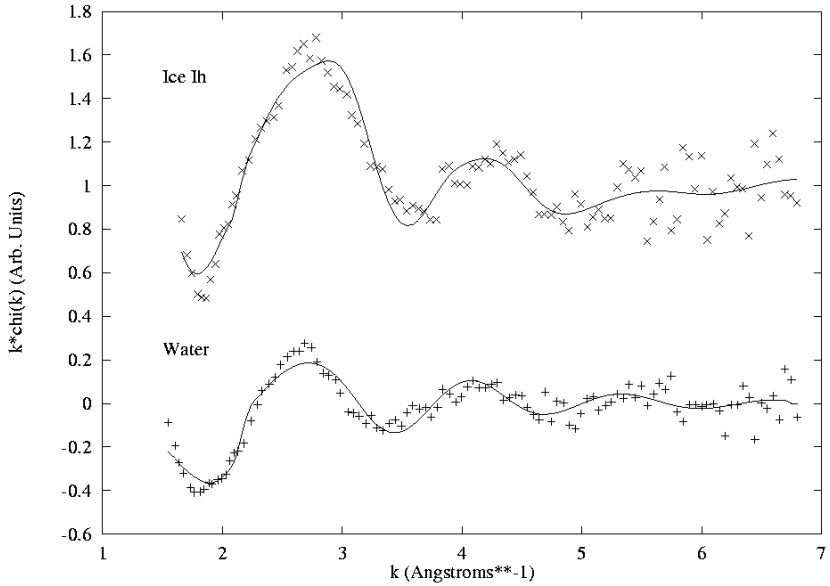

1) Analysis of Ice Ih IRS data using known structure of Ice Ih
2) Extraction of parameters that govern the distance scale and the coordination number.
3) Transfer of the parameters to the liquid state analysis.
4) Refinement of the liquid state IRS data.

EXAFS Analysis II

$$\chi(k) = \int_0^\infty 4\pi r^2 \rho\, g_2(r) A(k,r) \sin\left(2kr + \phi(k,r)\right) dr$$

$$\chi(k) = \left[\sigma(E) - \sigma_0^t(E)\right] / \sigma_0(E)$$

$\sigma_0^t(E)$: atomic contribution to absorption cross section

$\sigma_0(E)$: atomic cross section of selected absorption edge

O-O partial radial distribution function

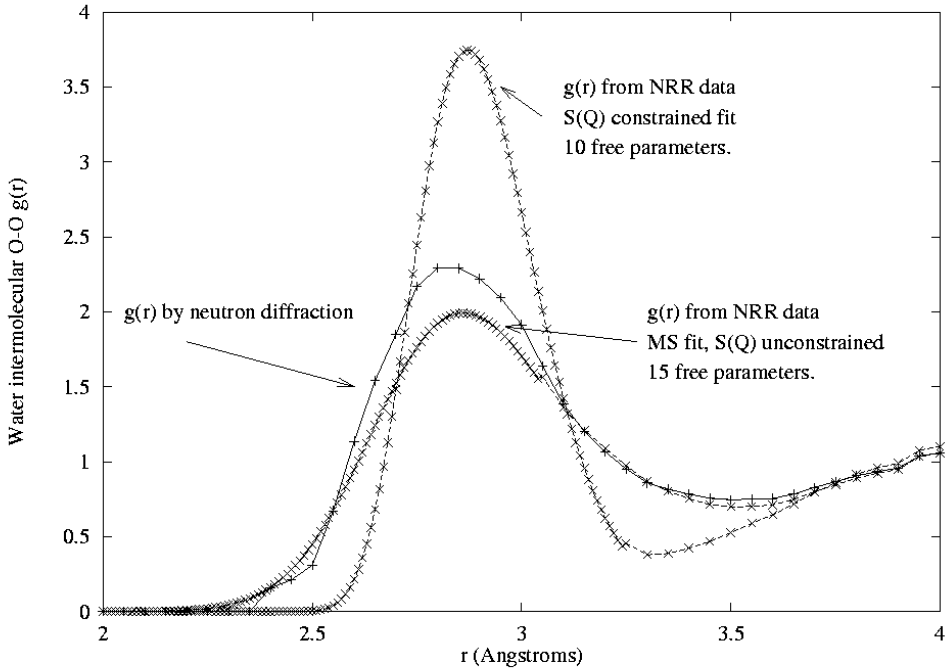

X-ray Raman Scattering:
O-O distance: 2.87 Å
Coordination: 4 - 7

Neutron Scattering:
O-O distance: 2.85 Å
Coordination: 4.4

XANES of the Oxygen K-edge in water

U. Bergmann et al.; Phys. Rev. B 66, 092107 (2002)

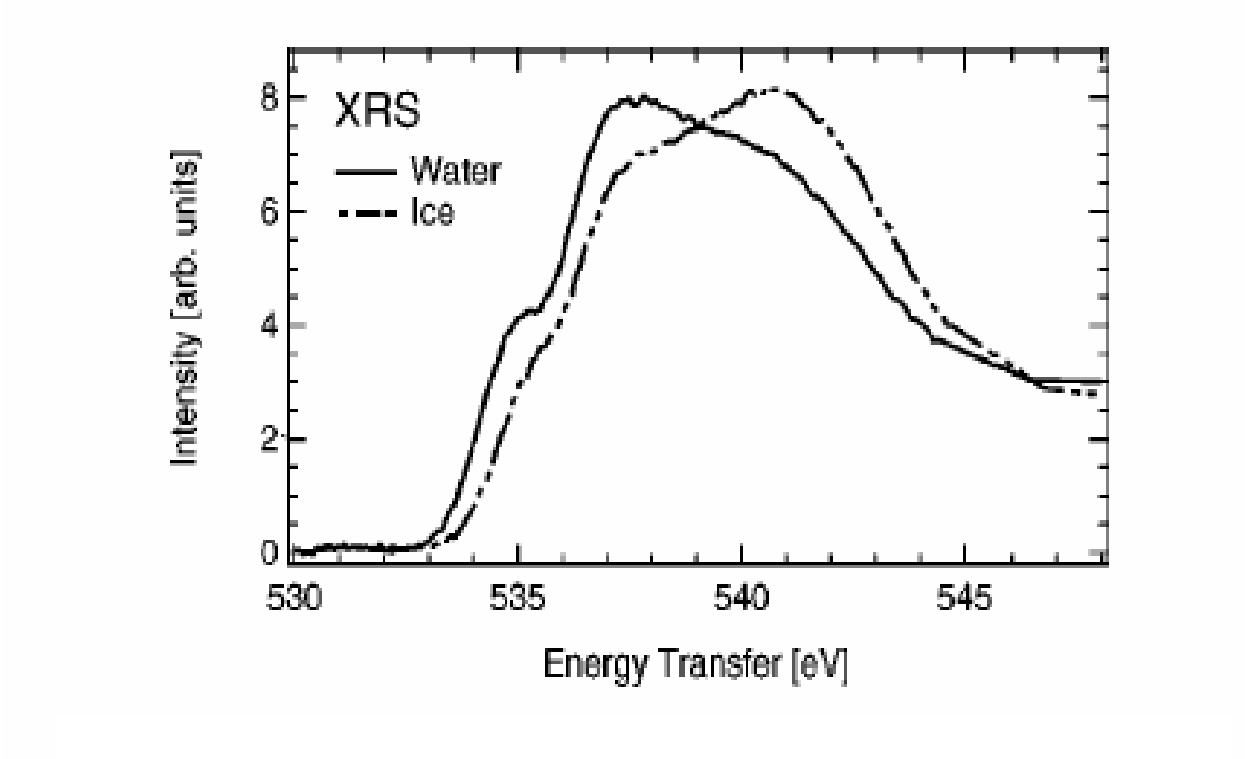

- XANES sensitive to the number of hydrogen bonds.
- Support by calculations.
- Analysis suggest significantly less than 3.5 H-bonds/molecule.

XRS from the O K-edge in ice II

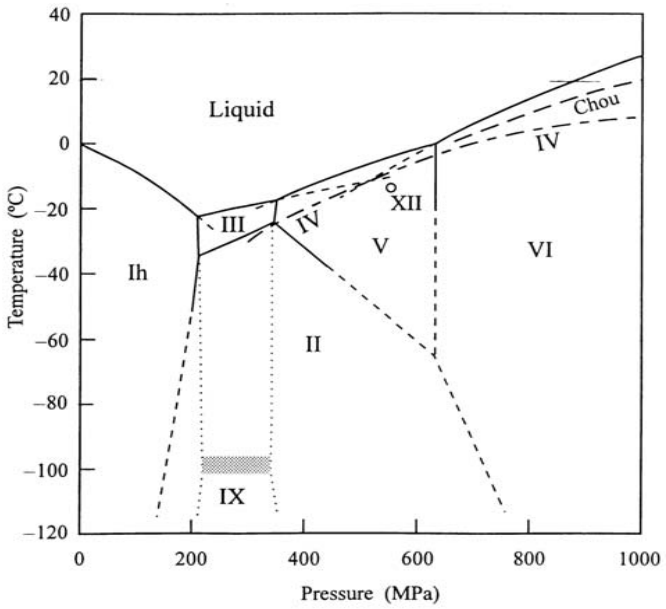

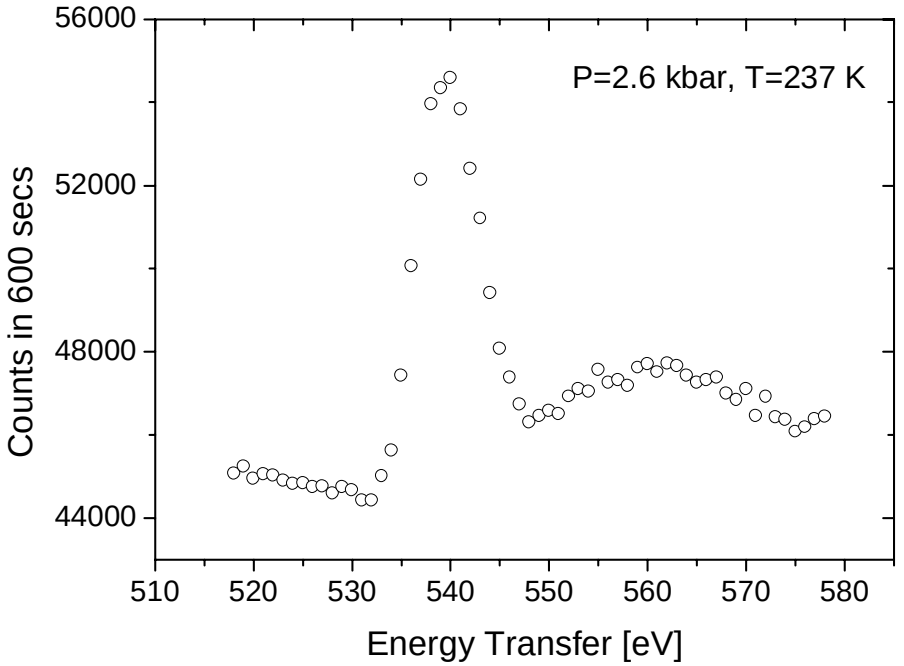

Large volume pressure cell
ΔE = 3.7 eV at 13.5 keV
12 hours accumulation

Strong reduction of contrast due to C K-edge EXAFS of diamond HP cell windows.

SUMMARY

Soft x-ray spectroscopy in the hard x-ray regime

- "simple" sample environment
- bulk sensitive
- access "exotic" final states
- extreme conditions: high temperature, high pressure

Weak probe

- practically limited to $Z < 14$
- limited quality for structural analysis (EXAFS)
- reasonable quality in the XANES region
- for high T, P measurements: cell window contribution critical

Exploit information contained in the near-edge region.

Resonant inelastic x-ray scattering

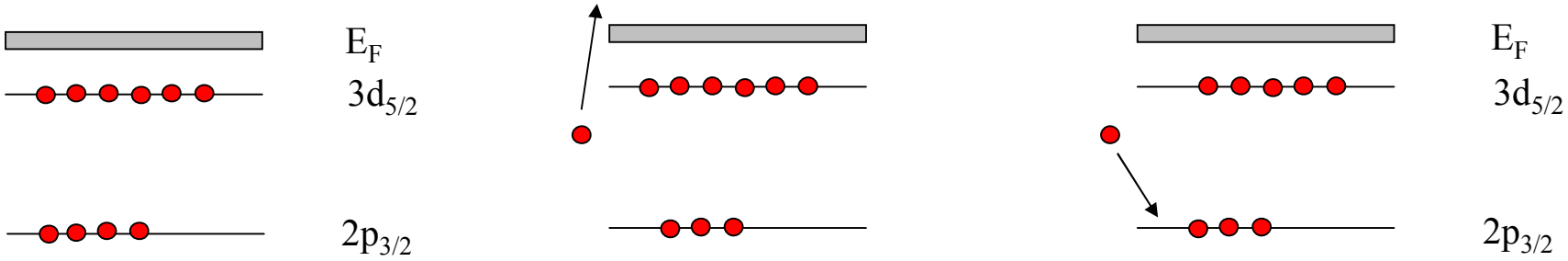

$$E_{2p} + e_k = \hbar\omega_1 \qquad E_{3d} + e_k = \hbar\omega = \hbar\omega_1 - \hbar\omega_2$$

Emission Absorption

$$\frac{d^2\sigma}{d\hbar\omega_2 d\Omega} \approx \sum_f \left| \sum_n \frac{\langle f | C_{q'}^{(m)} | n \rangle \langle n | C_q^{(m)} | i \rangle}{E_i - E_f + \hbar\omega_1 - i\Gamma_n} \right|^2 \delta\left(E_f - E_i - \hbar\omega\right)$$

Resonant denominator

Resonant Inelastic X-ray Scattering

Er L_3 ($2p_{3/2}$) edge

decay channel:
$3d_{5/2} \rightarrow 2p_{3/2}$

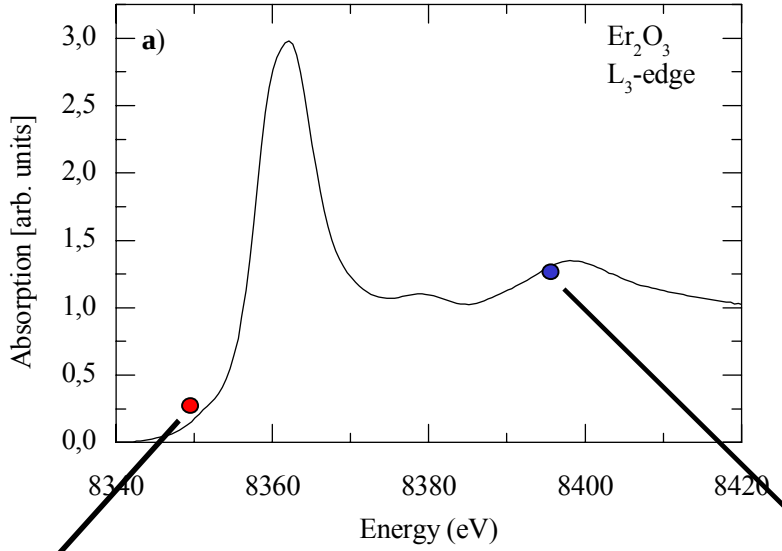

Spectral resolution limited by Γ_{2p}

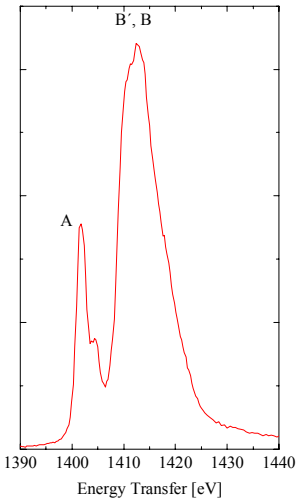

Spectral resolution limited by Γ_{3d}

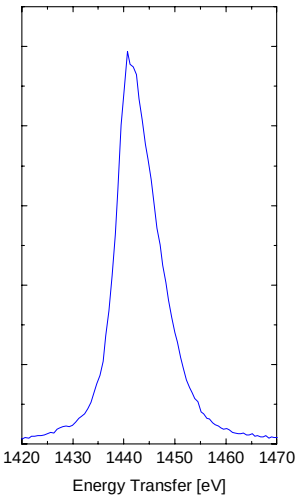

Constant Final State Scans

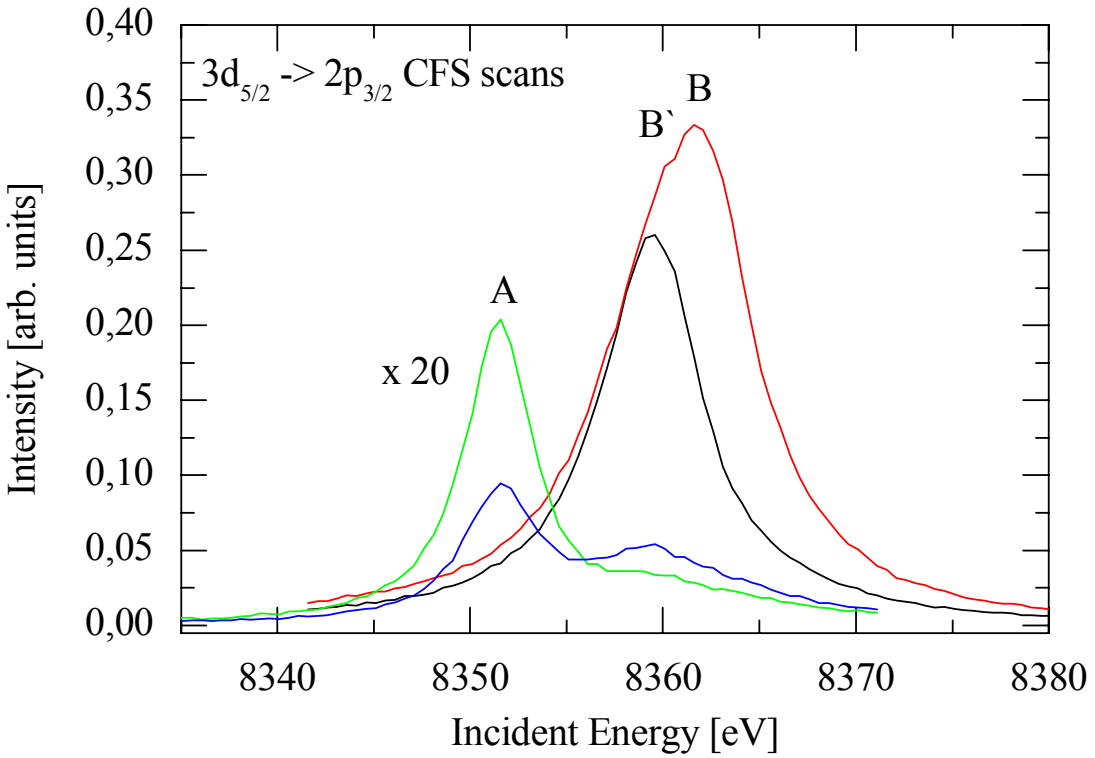

B and B*: 2p→5d dipolar transitions
different intermediate states, cubic field splitting of the 5d states: $\Delta E = 2.3$ eV

A and A*: 2p→4f quadrupolar transition
Same intermediate state, splitting due to spread of final state multiplet.

Conclusions

RIXS allows the separation of different excitation channels which are obscured in a standard absorption measurement.

Condition:

Final state core-hole lifetime
<
energy separation of the multiplet families

RIXS at the L_3-edge of Yb in $YbInCu_4$ and $YbAgCu_4$

C. Dallera et al.; Phys. Rev. Lett. 88, 196403 (2002)

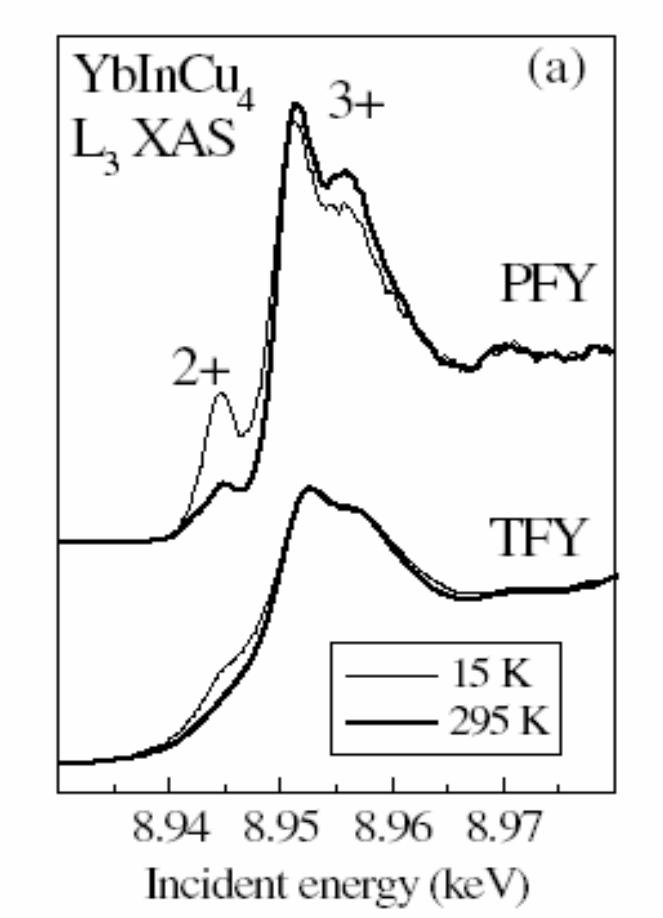

Mixed valence ground state

Yb^{3+}: $4f^{13}$

Yb^{2+}: $4f^{14}$

RIXS:
Enhancement of spectral contrast

Schematics of the RIXS 2p3d RIXS process

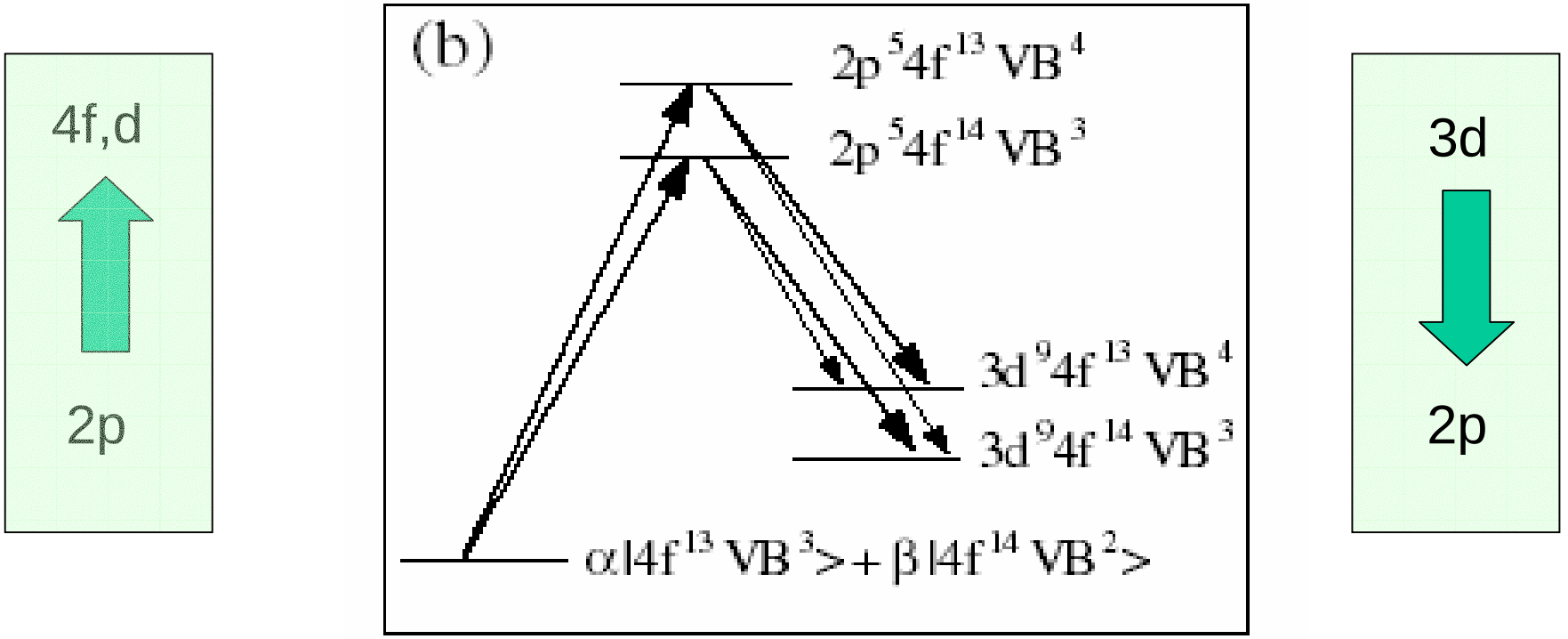

Dipolar excitations: $2p^6 4f^{13} VB^3 \rightarrow 2p^5 4f^{13} VB^4$

Quadrupolar excitations: $2p^6 4f^{13} VB^3 \rightarrow 2p^5 4f^{14} VB^3$

The resonant enhancement of the $2p^5 4f^{14}$ intermediate state

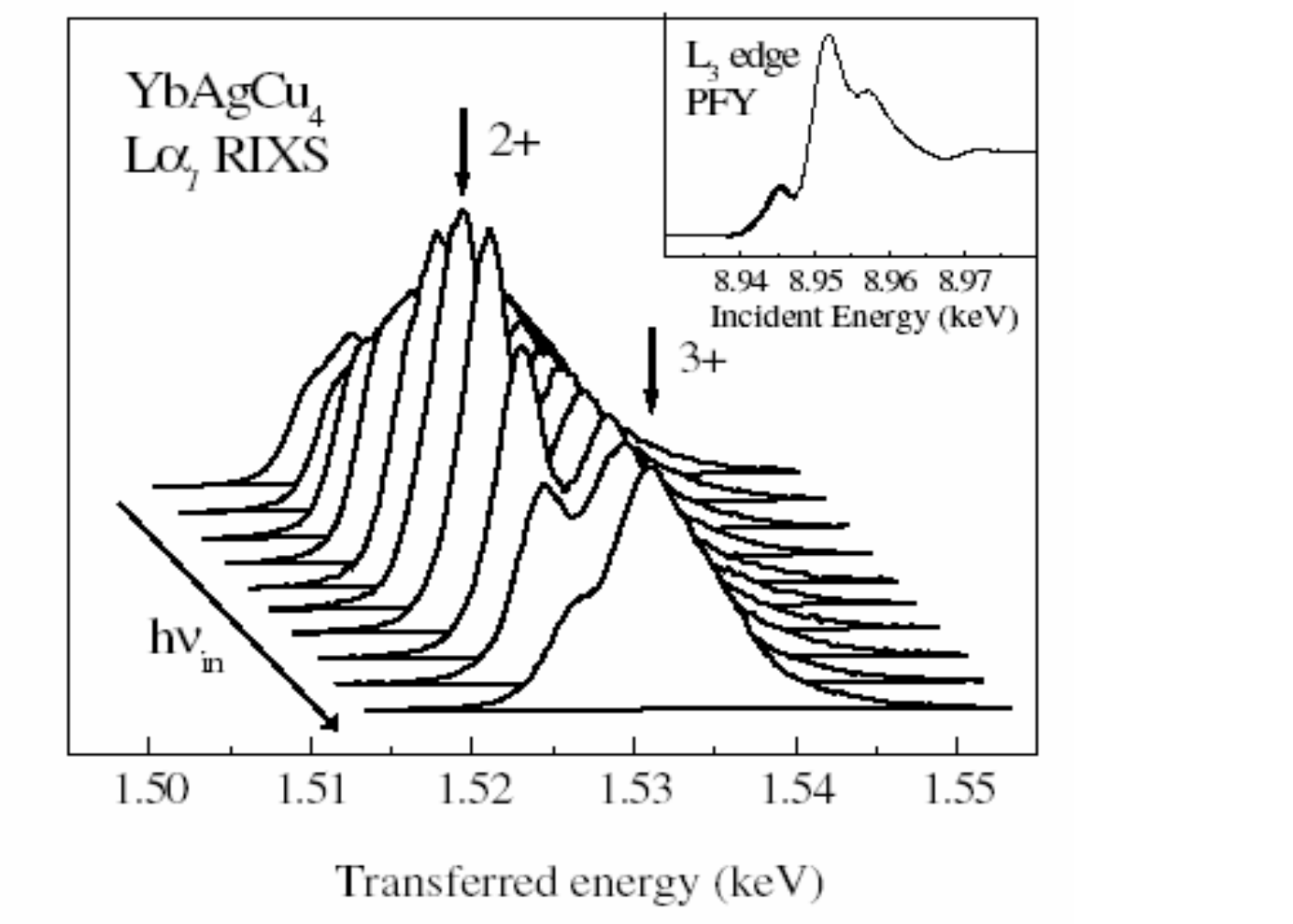

Temperature dependence of the $3d^9 4f^{14}$ final state multiplet

Sudden valence change

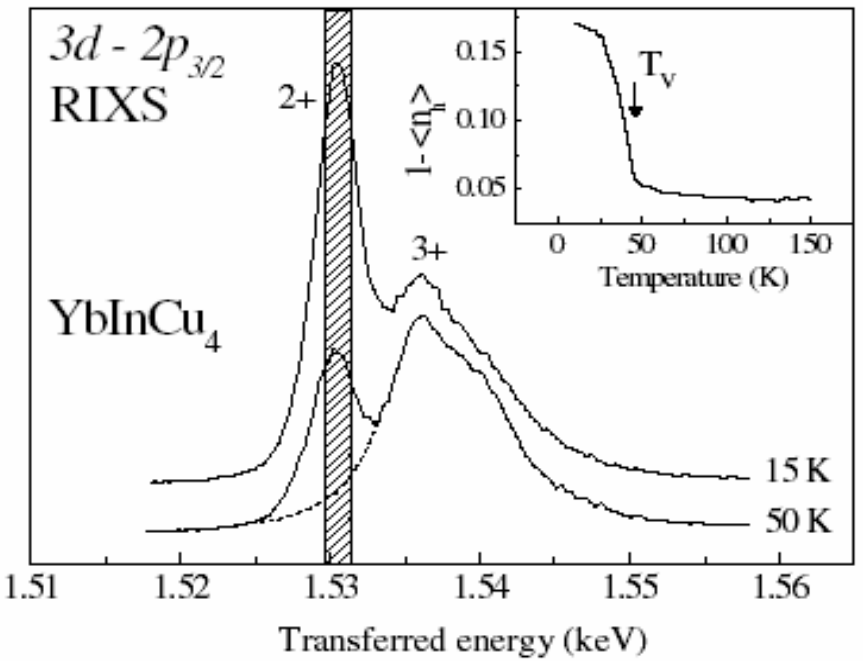

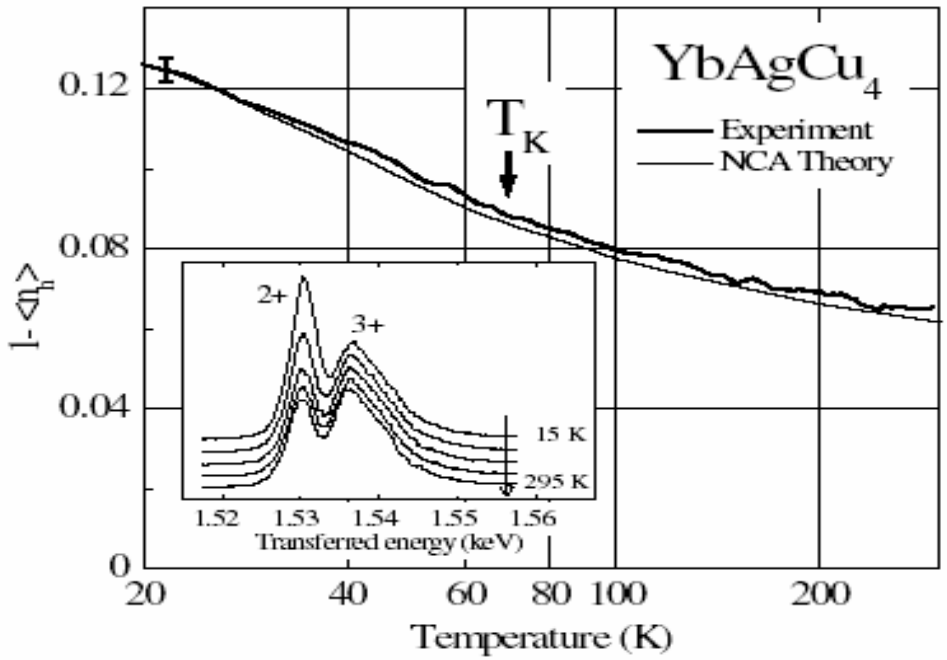

Smooth valence change

Partial Fluorescence Yield Absorption Spectroscopy

- Spectral sharpening by energy selection of radiative decay channel.
- E_{scatt} fixed, E_{inc} tuned through absorption edge.

Pt $L\beta_2$ emission line: $4d \rightarrow 2p_{3/2}$

Pt L_3-edge

$\Gamma_{L3} = 7$ eV

$\Gamma_{M4,5} = 1.9$ eV

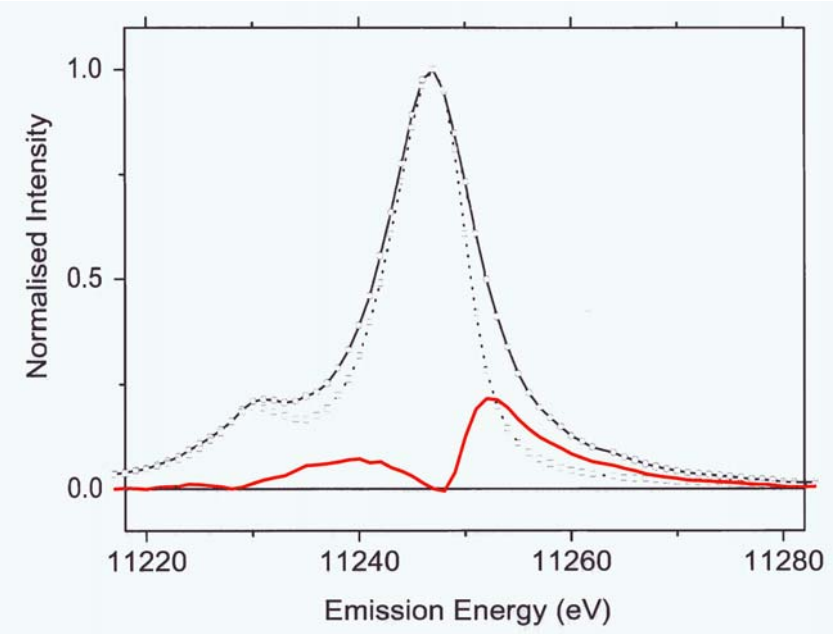

XAS L_3 edge of Pt metal

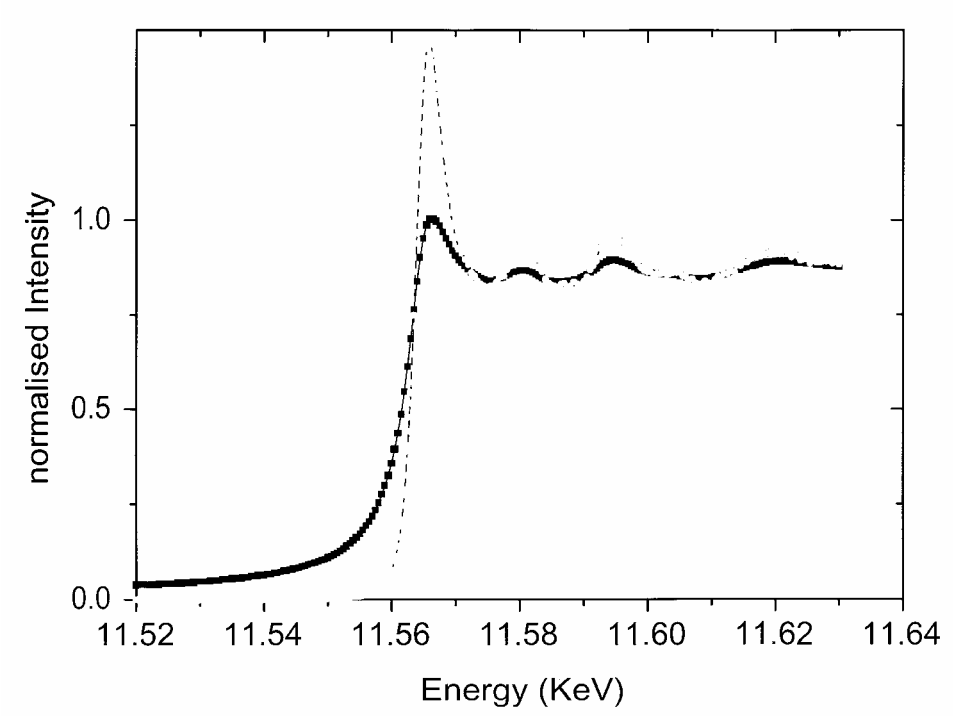

$$1/\Gamma_{PFY} = \sqrt{1/\Gamma_{2p}^2 + 1/\Gamma_{4d}^2}$$

Significant spectral sharpening !!!

High resolution X-ray Fluorescence

element

angular momentum

Fe 3p -> 1s radiative decay

valence (energy position)

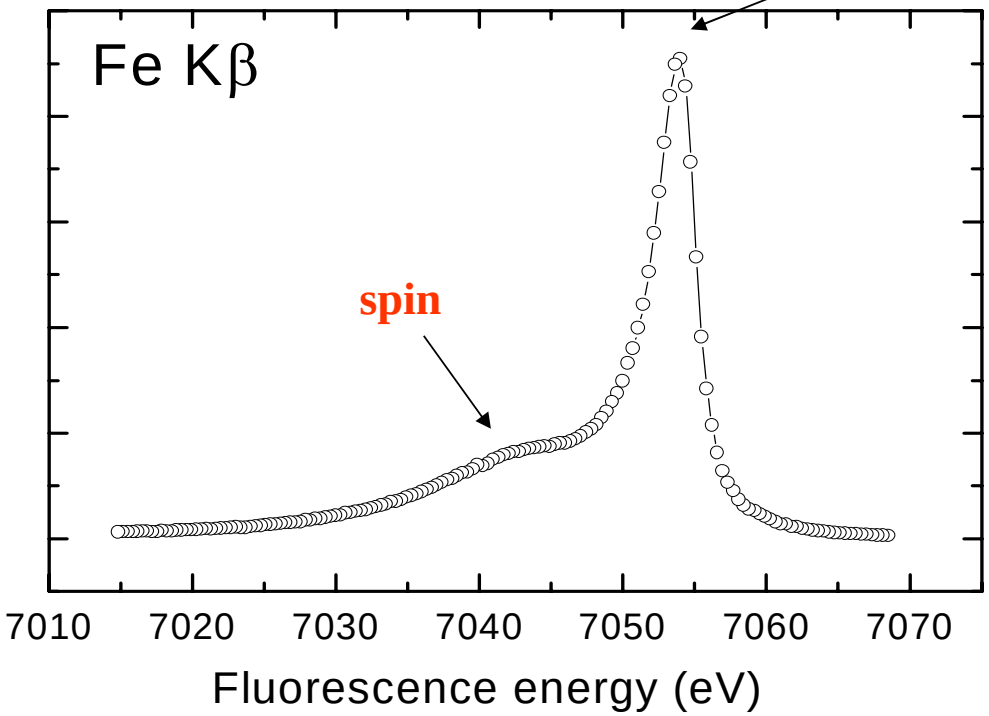

The pressure induced magnetic phase transition in iron metal.

Diamond Anvil cell

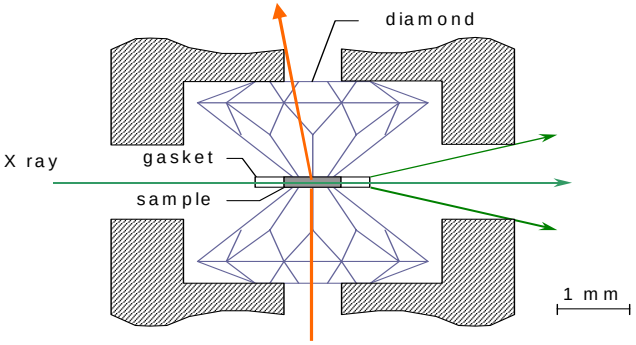

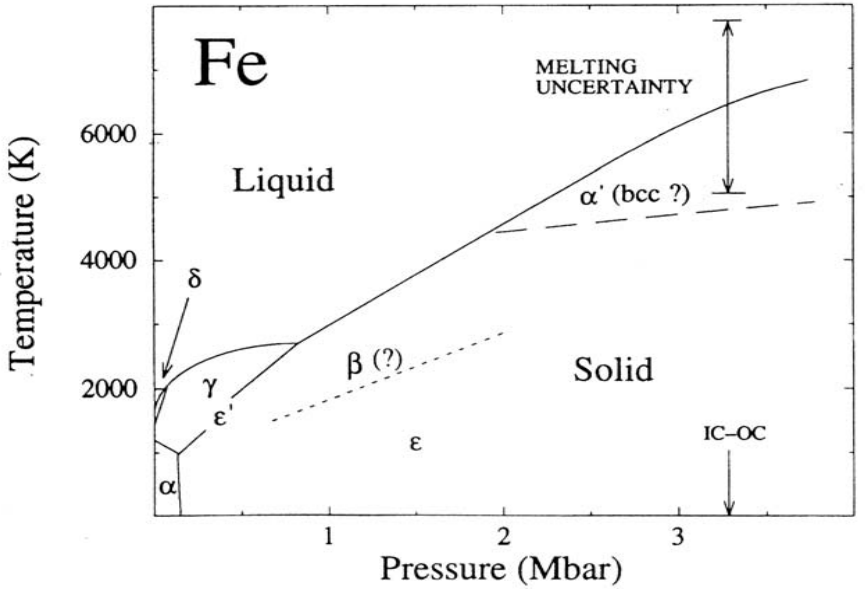

- small beam: 50-100 μm
- high flux
- X-ray diffraction as diagnostics tool

α (bcc) -> ε (hcp) bei 13 GPa

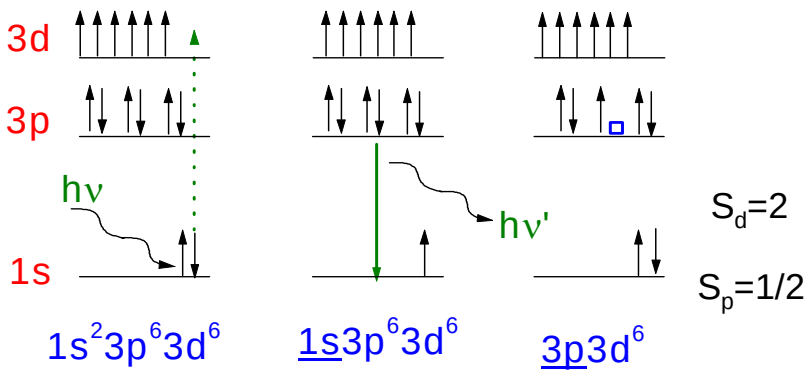

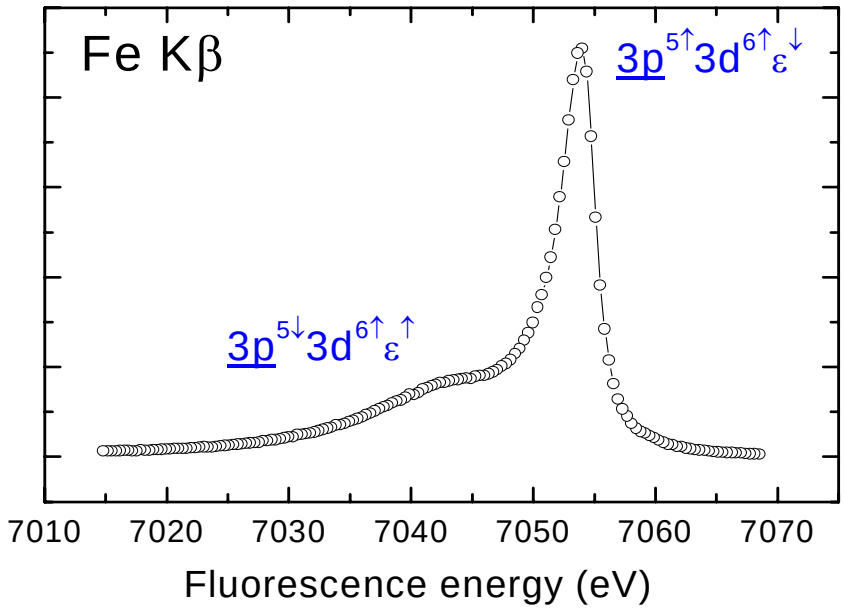

•Satellite structure arises from Coulomb- and exchange interactions between the 3p- and the 3d electrons.

- Main line: $S_d = 2$; $S_p = 1/2$, $e_{\downarrow}$ => spin-down character

- Satellite: $S_d=2$; $S_p= -1/2$, $e_{\uparrow}$ => spin-up character

Evidence magnetic phase transition through changes in emission line shape.

- intraatomic probe of the size of the 3d magnetic moment
- fast time scale: 10^{-15} s
- ferro-, antiferro-, ferri- and paramagnetic systems

Complementary to:

- X-ray magnetic circular dichroism (XMCD)
- Mössbauer spectroscopy

Pressure-induced ferromagnetic to non-magnetic transition in iron metal

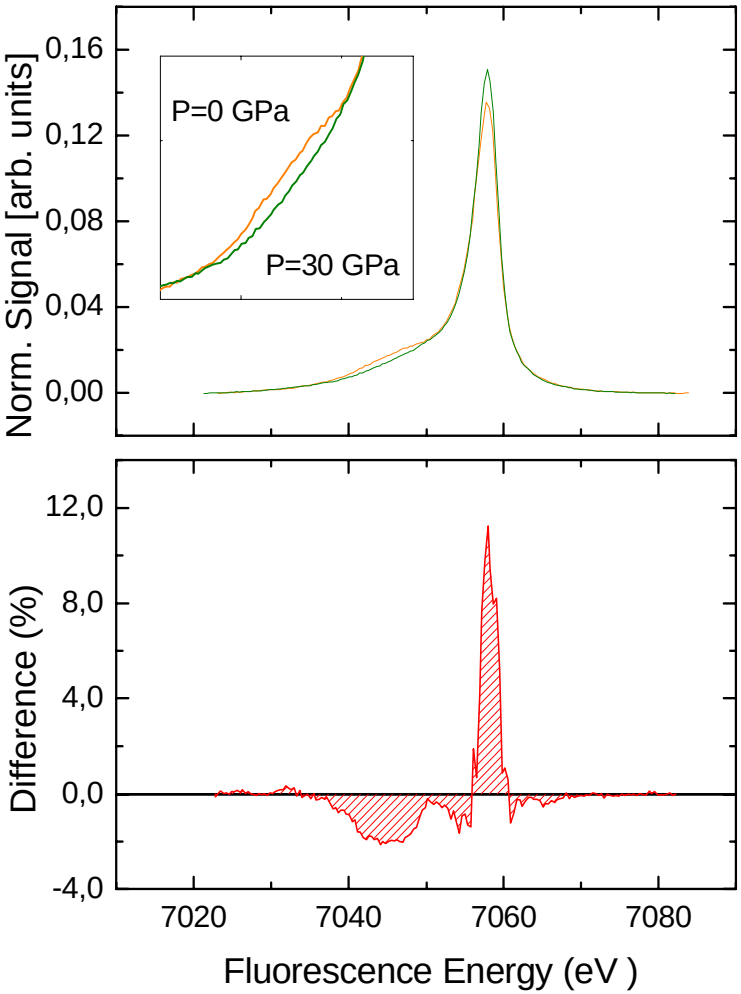

Simplified picture of the exchange split 3d- band

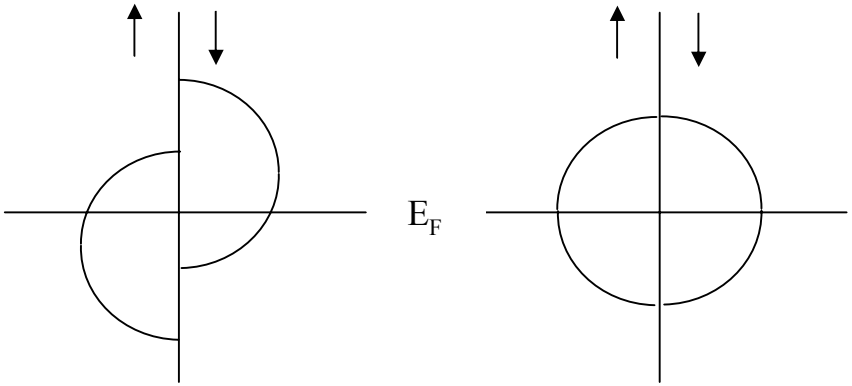

ferromagnetic

non-magnetic

Ferromagnetic to non-magnetic transition in iron metal

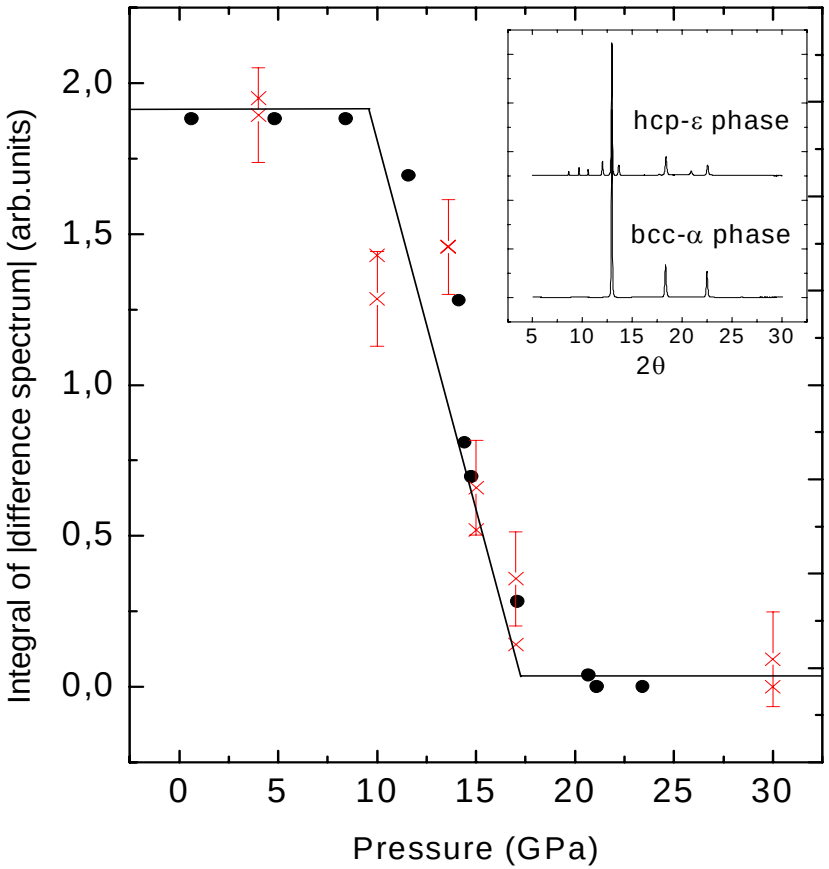

- Transition at about 13 GPa.
- Good agreement with Mössbauer and diffraction data.

Magnetism of FeNi Invar alloy under pressure

J.P. Rueff et al.; Phys. Rev. B 63, 132409 (2001)

Fe Kβ-emission of $Fe_{64}Ni_{36}$ Invar

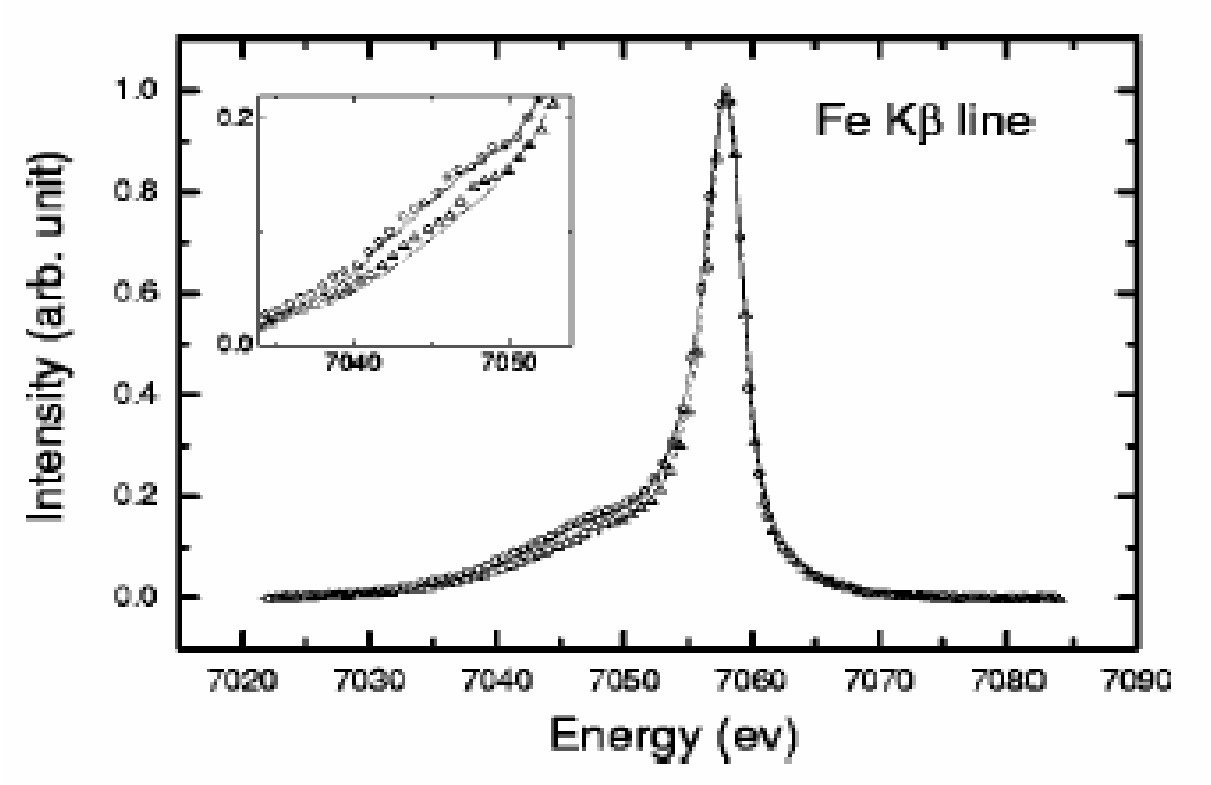

The difference spectra

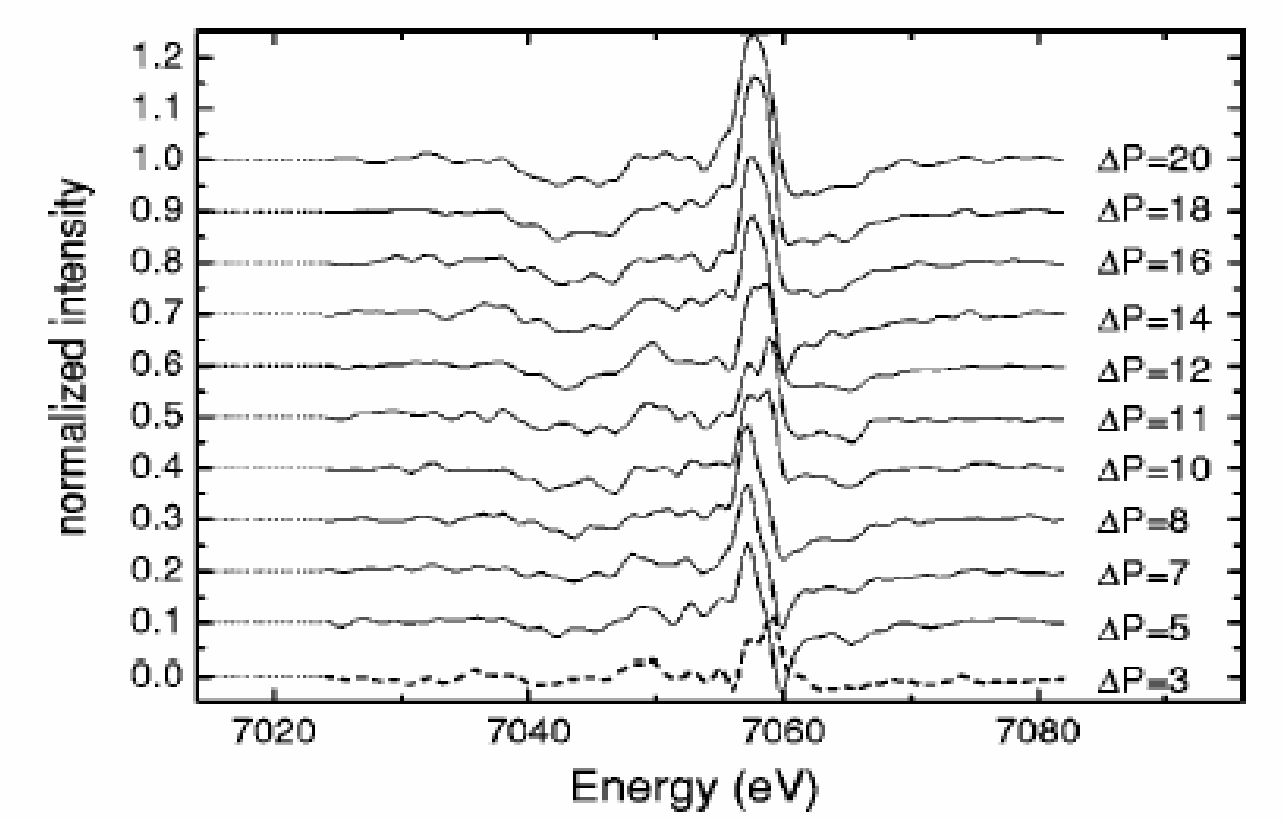

Pressure evolution of the spin moment

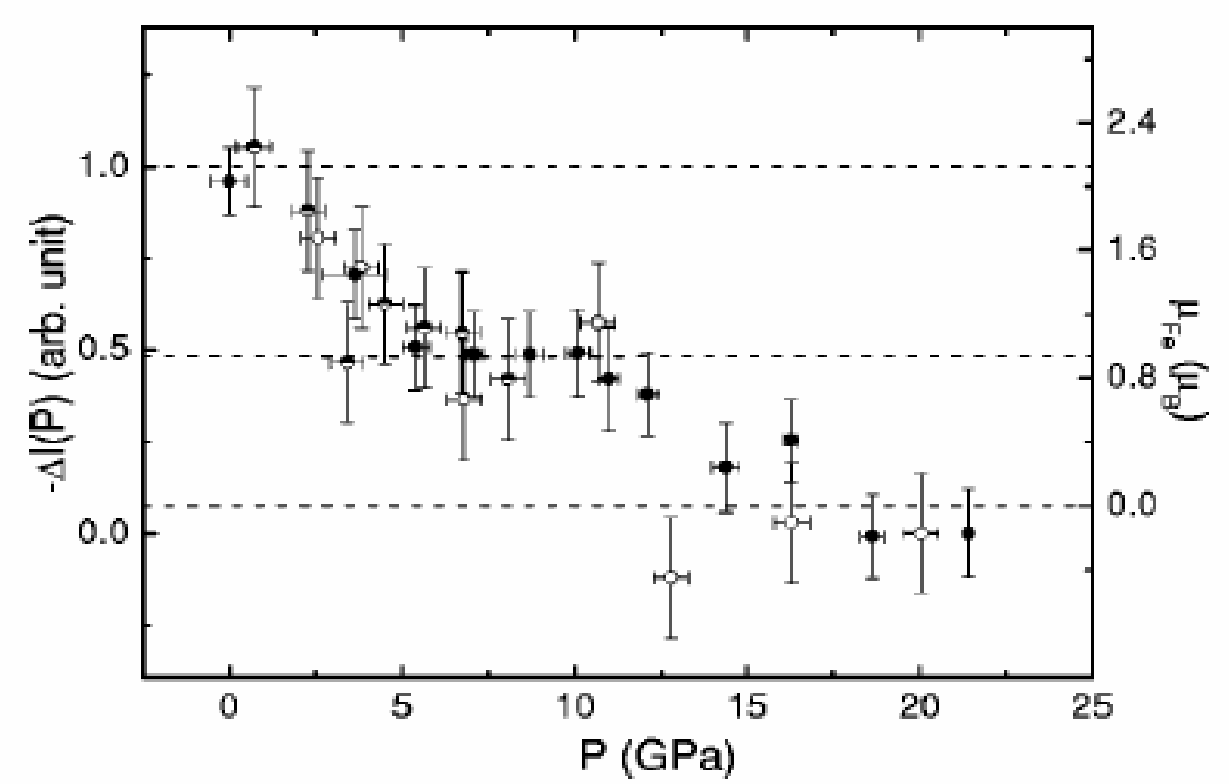

- Existence of an intermediate spin state.
- Non-magnetic state above 15 GPa.
- Agreement with recent predictions.